


Accuracy Assessment of the ICESat-2/ATL06 Product in the Qilian Mountains Based on CORS and UAV Data

Yanli Zhang , Senior Member, IEEE, Yan Pang, Dudu Cui, Yupeng Ma, and Linhong Chen, Member, IEEE

Abstract—Ice, Cloud and Land Elevation Satellite-2/Advanced Topographic Laser Altimeter System 06 (ICESat-2/ATL06) data can be widely used for various applications, such as monitoring changes in glacier thickness. In this article, we use field surveys based on continuously operating reference system (CORS) and unmanned aerial vehicles (UAVs) to verify the elevation accuracy of the ATL06 product. A total of 208 ATL06 footprints were selected for an accuracy assessment by obtaining 348 CORS global positioning system (GPS) measurements and deriving a digital elevation model (DEMs) from 2683 UAV images in four experimental areas with different terrain and landform types in the Qilian Mountains, China. The experiments show that ATL06 data have very high vertical accuracy and horizontal positioning accuracy; the average root-mean-square error (RMSE) yielded by CORS is 0.0846 m, and the corresponding RMSE yielded by the UAV data is 0.1517 m. Furthermore, the positioning accuracy was also affected by the terrain slope.

Index Terms—Advanced topographic laser altimeter system (ATLAS), digital elevation model (DEM), geoscience laser altimeter systems (GLAS), stereo model, vertical elevation accuracy.

I. INTRODUCTION

THE geoscience laser altimeter systems (GLAS) spaceborne laser altimeter carried by Ice, Cloud, and Land Elevation Satellite-1 (ICESat-1) was successfully launched in January 2003, and its main task is to measure the ice mass balance, cloud and aerosol heights, and land topography and vegetation characteristics [1]–[4]. ICESat-1/GLAS products include ice sheet (GLA12), ocean (GLA15), and land (GLA14) products, which can be widely used in various fields. Some researchers have explored ice sheet elevation changes in the north and south in the past decade based on ICESat-1/GLAS products [5]–[8]. DiMarzio *et al.* [9] generated Antarctica digital elevation models (DEMs) with a 500-m spatial resolution and Greenland DEMs with a 1-km spatial resolution for monitoring the volume variation in ice sheets from February 2003 to June 2005.

Manuscript received July 3, 2020; revised November 12, 2020; accepted December 3, 2020. Date of publication December 14, 2020; date of current version January 8, 2021. This work was supported in part by the National Natural Science Foundation of China (NSFC) Project under Grant 41871277 and Grant 41561080, and in part by the China Postdoctoral Fund Project under Grant 2016M602893. (Corresponding author: Yanli Zhang.)

The authors are with the College of Geography and Environment Science, Northwest Normal University, Lanzhou 730070, China (e-mail: zyl0322@nwnu.edu.cn; 2018222391@nwnu.edu.cn; 2017212200@nwnu.edu.cn; 2019212418@nwnu.edu.cn; 2018212329@nwnu.edu.cn).

Digital Object Identifier 10.1109/JSTARS.2020.3044463

ICESat-1/GLAS has been used to verify the vertical accuracy of different DEM products, such as the shuttle radar topography mission (SRTM) DEM, advanced spaceborne thermal emission and reflection radiometer (ASTER) DEM, and advanced land observation satellite (ALSO) DEM [10], [11]. Some studies have estimated vegetation height and identified forest species in various regions based on ICESat-1 and Landsat data [12]. Indirabai *et al.* [13] pointed out that the forest canopy height and the structural properties can be accurately estimated by ICESat-1/GLAS data. Furthermore, with the ICESat-1/GLAS data, the variation in the water level can be detected for many years [14], [15].

However, ICESat-1 stopped working in 2009 due to the loss of the laser sensor [16]. The IceBridge initiated by National Aeronautics and Space Administration (NASA) provides a bridge in terms of remote sensing data between ICESat-1 and the upcoming ICESat-2 in polar regions from 2009 to 2019. However, IceBridge observations are limited in terms of regional and temporal distributions. Fortunately, the ICESat-2 satellite equipped with an advanced topographic laser altimeter system (ATLAS) was launched in California in September 2018. It provides repeat altimetry measurements not only for the cryosphere but also for land, vegetation, inland water, the sea surface, cloud layers, and optical thickness [17]. The ICESat-2/ATLAS mission has released various products, including land ice (ATL06), sea ice (ATL07), vegetation (ATL08), atmosphere (ATL09), ocean (ATL12), and inland and water (ATL13) products [18]–[20]. Compared with GLAS, the ATLAS instrument has the advantages of the rapid acquisition of higher precision elevation, improved spatial resolution, and the ability to measure a cross-track slope. Currently, ICESat-2/ATLAS products have been applied to many different disciplines of research. Some studies have combined ICESat-1/GLA14, ICESat-2/ATL13, and Landsat data to estimate the changes in the lake level and volume on the Tibetan Plateau [21]. Neuenschwand *et al.* [22] used airborne lidar data to verify the accuracy of ATL08. Considering its advanced altimetry technology, the ICESat-2 ATL06 product is expected to have several advantages in elevation monitoring. However, few studies have evaluated the performance of ATL06 data in the Qilian Mountains.

Currently, various methods have been used to evaluate the reliability of vertical elevation accuracy, including traditional geodetic measurements, global positioning system/global navigation satellite systems (GPS/GNSS) differential techniques,

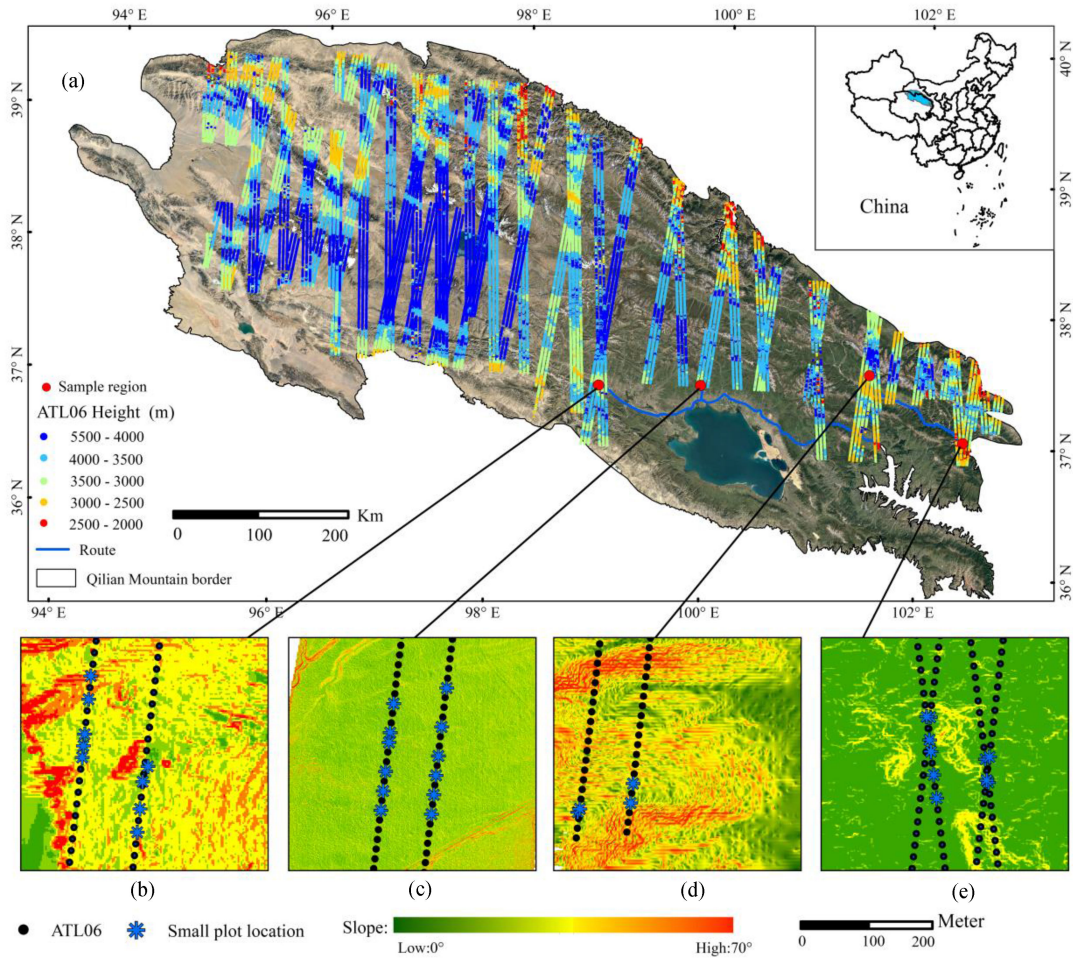


Fig. 1. Details of the CORS sample plots in the Qilian Mountains and the four experimental areas. (a) Location of the study area and the footprints of ICESat-2/ATL06 data. (b) Qinggangxia. (c) Menyuan. (d) Gangcha. (e) Tianjun.

GNSS continuously operating reference station (CORS), and aerial photogrammetry. Traditional height geodetic instruments include level gauges and theodolites, etc., which have high accuracy and reliability for a small area of local terrain [23]. However, these geodetic methods require considerable manpower and material resources and need more accurate ground control points (GCPs), which makes measurements inefficient. In addition, data processing is relatively large and difficult to carry out [24]. GPS/GNSS differential measurement is simple and convenient, but it also requires a considerable number of GCPs to improve the accuracy of surface elevation measurements. The CORS measurement uses a combination of GNSS, computers, data communications, and Internet technologies, and can achieve centimeter-level positioning and navigation without the need for users to build GCP networks [25]. Nevertheless, both GPS and CORS measurements are a point-measured method that can only measure the coordinates of one point at a given time. Photogrammetry is a surface-measured method that can generate stereo model pairs of images to obtain synchronously large area surface heights. In recent years, the unmanned aerial vehicles (UAVs) have become an important means to extract quickly DEM data due to its flexibility, higher spatial and temporal resolutions [26]–[29]. The vertical surface

elevation accuracy derived from UAVs can reach the centimeter level [30]–[32].

Therefore, in this research, the CORS and UAV measurements are selected to evaluate the vertical elevation accuracy of ICESat-2/ATL06 products in four experimental plots in the Qilian Mountains. The study is organized as follows. Section II describes the study area and data. Section III introduces an integrated approach to evaluate the ICESat-2/ATL06 product. Section IV presents the verification results, and Section V discusses the results. Finally, Section VI concludes this article.

II. STUDY AREA

A. Study Area

As shown in Fig. 1, the study area lies in the Qilian Mountains ($94^{\circ}10'–103^{\circ}04'E$, $35^{\circ}50'–39^{\circ}19'N$), which is located at the northeastern margin of the Tibetan Plateau, mainly in Qinghai and Gansu Provinces. The area is 10 400 km², which spans approximately 850 km from west to the east and 200–400 km from north to south. The terrain of the Qilian Mountains is complex with elevations from 1500 to 6000 m above the sea level, and the major land cover types include grassland, cropland, and bare land. The Qilian Mountains are an important ecological

TABLE I
BASIC INFORMATION OF THE FOUR EXPERIMENTAL AREAS

	Location	Elevation (m)	Land cover type	Slope (°)
Qinggangxia	37°2', 102°24'	2329.47-2424.36	Grassland	0-30
Menyuan	37°31', 101°30'	3158.36-3421.42	Cropland and grassland	0-25
Gangcha	37°23', 99°53'	3302.97-3438.35	Low-coverage bare land and grassland	0-65
Tianjun	37°19', 98°55'	3429.45-3449.46	Low-coverage grassland	0-10

TABLE II
BASIC INFORMATION ON THE ICESat-2/ATL06, UAV, AND CORS MEASUREMENTS IN THE FOUR SUBAREAS

Experimental areas	Date	GVPs	ICESat-2/ATL06		UAV		
			Footprint points	Overpasses	Flight altitude (m)	Images	GCPs
Qinggangxia	2019.8.11	13 (98)	40	2018.11.27	80	473	14
Menyuan	2019.8.12	14 (95)	48	2019.1.26	80	841	16
Gangcha	2019.8.13	7 (50)	41	2018.11.04	100	125	9
Tianjun	2019.8.14	16 (105)	79	2018.10.23, 2019.01.09	80	1244	17
Total		50 (348)	208			2683	56

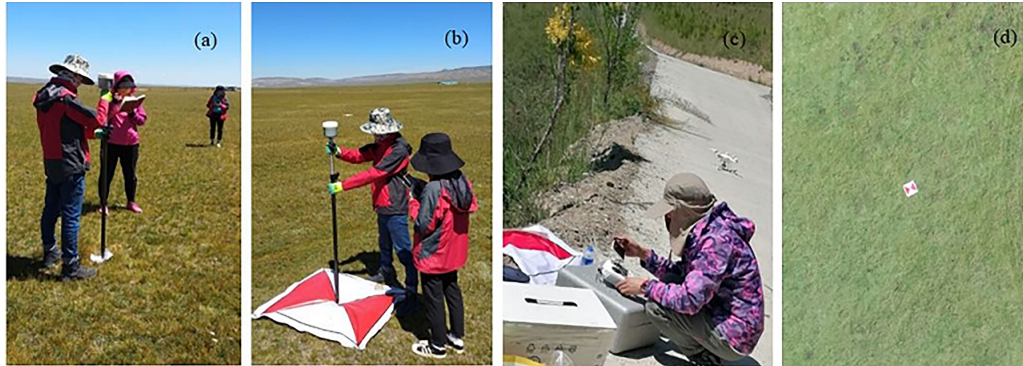


Fig. 2. CORS measurements and UAV mapping. (a) GVPs. (b) GCPs. (c) UAV flight scene. (d) GCP captured by UAV images.

security barrier in the western region of China and an important base for the protection of biodiversity in China [33].

Four experimental areas with convenient accessibility were selected for CORS ground surveys and UAV flights in the southeastern region of the Qilian Mountains (see Fig. 1). The elevation of the experimental area is approximately 2300–3300 m, and the average area of each measurement area ranges from approximately 0.25 km². The experimental subareas are as follows: Qinggangxia, which is mainly covered with grassland and has terrain with a relatively high slope; Menyuan, which is mainly covered with cropland and grassland and has relatively flat terrain; Gangcha, which is covered with grassland and bare land with low vegetation coverage and has relatively complicated terrain; and Tianjun, which is mainly covered with sparse grassland and has very flat terrain. The basic information on the four experimental subareas is described in Table I.

III. DATA AND METHOD

A. Data

The main data used in this article include the ICESat-2/ATL06 product, CORS measurements, and UAV images. The ATL06 data are derived from the level-3 product of ICESat-2, which is

provided by the National Snow and Ice Data Center (NSIDC) since September 2018 available for download.¹ The field CORS measurements and UAV images were obtained to evaluate the elevation accuracy of ICESat-2/ATL06. The values of the three elevation datasets were ultimately calibrated to the World Geodetic System 1984 (WGS84) ellipsoid, and the detailed information on the four experimental areas is described in Table II. It should be noted that the CORS measurements have two purposes. One is to provide ground verification points (GVPs) to directly validate the accuracy of the ICESat-2/ATL06 product, and the other is to provide GCPs for UAV mapping to construct an accurate 3-D surface. Basic information on the ICESat-2/ATL06, UAV, and CORS measurements in the four subareas is shown in Fig. 2.

1) *ICESat-2/ATL06 Product*: The ICESat-2/ATL06 product provides a time series of land-ice surface heights at a given time and location. Six laser beams of ATLAS scan the Earth's surface at a small angle, forming a rectangular array footprints of 2 rows and 3 columns (separated by 3.3 km) on the ground. Thus, ATLAS consists of three pairs of laser pulses, including a weak beam and a strong beam, each pair separated by 90 m in the vertical orbit direction, as shown in Fig. 3. The ATL06

¹ [Online]. Available: <https://icesat-2.gsfc.nasa.gov/>

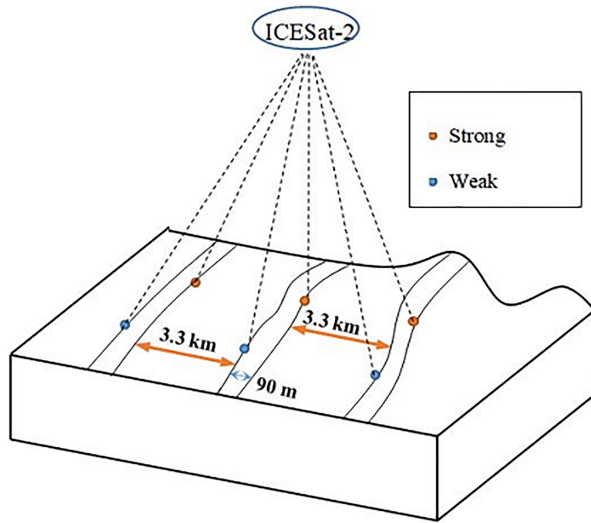


Fig. 3. Schematic diagram of the ICESat-2 data operation. The red dots indicate strong beams, and blue dots indicate weak beams.

measurements at a given point provide the geodetic latitude, longitude, and height above the ellipsoid using the WGS 84 geographic coordinate system (ITRF2014 reference frame) [34]. In addition, the ATL06 product also provides some auxiliary data, such as instrument parameters, quality of height estimates, and other metadata, which are packaged along with altimeter data and stored as hierarchical data format (hdf5) files.

From October 2018 to February 2019, there are 65 scanning tracks of ICESat-2/ATL06 in the Qilian Mountains (see Fig. 1). In the 4 experimental areas, 5 scanning tracks crossover, and 208 surface footprints are selected for elevation accuracy evaluation. Detailed information on ATL06 in each test area can be described in Table II.

2) *CORS Measurements*: Before the experiment began, we purchased a one-month CORS service on the official CORS website. Using the CORS service account, 3-D coordinates of a given surface were collected by the differential positioning principle of the GPS receiver, and their accuracies reached a few centimeters both horizontally and vertically. During this field verification test, the GPS receiver of CHCNAV i80 GNSS was selected. A total of 336 CORS GVPs were measured from August 11, 2019 to August 16, 2019, in the four experimental areas of the Qilian Mountains: 101 CORS GVPs were measured in Qinggangxia, 70 CORS GVPs were measured in Menyuan, 59 CORS GVPs were measured in Gangcha, and 106 CORS GVPs were measured in Tianjun, as described in Table II. Furthermore, 56 GCPs measured by CORS were also collected for UAV mapping.

3) *UAV Survey*: In this experiment, a lightweight UAV, a DJI Phantom 4 RTK (real-time kinematic) was selected to derive high-resolution DEM. Flight planning and launching utilized the GS RTK mobile app preinstalled on the RTK controller. The HxGN SmartNet (a precise positioning service) corrections network subscription is purchased on the DJI official website.² The RTK mode is recommended to enable the RTK module

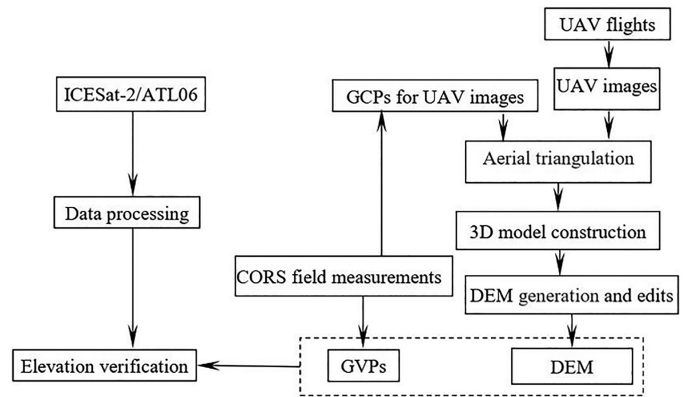


Fig. 4. Flowchart of the accuracy verification of the ICESat-2/ATL06 product using CORS and UAV measurements.

to receive RTK signals (American GPS, Chinese BeiDou, and European Galileo) via a 4G connection, which can provide real-time, centimeter-level absolute positioning accuracy. The ground sample distance (GSD) of the aerial photograph can be calculated by $H/36.5$ cm/pixel, where H (m) indicates the relative altitude of the aircraft. The camera loaded on the Phantom 4 RTK comprises 1 in of the complementary metal-oxide semiconductor (CMOS), 20 M effective pixels, 84° field of view (FOV), and a lens of 8.8 mm/24 mm. Detailed technical parameters of the Phantom 4 RTK can be found on the DJI official website.

In general, the official website claims that the mapping accuracy of DJI Phantom 4 RTK can meet the requirements of accuracy standards for digital orthophotos class III of the American Society for Photogrammetry and Remote Sensing (ASPRS) without GCPs. However, to increase the accuracy of the RTK imagery, some GCP marks or obvious features on the natural surface were measured by CORS surveys [see Fig. 2(b)]; such features must be easy to identify in the images [see Fig. 2(d)]. Four UAV flight areas were designed in the Qilian Mountains, and the GSD of all photos captured by the UAV was within 3.0 cm/pixel. The heading overlap and side overlap were 80% and 70%, respectively. Detailed information of the four UAV flight plots is as follows (see Table II).

- 1) The UAV flight altitude was set to 80 m, 473 photos were collected, and 14 GCPs were measured during the UAV overpasses in Qinggangxia.
- 2) The UAV flight altitude was set to 80 m, 841 photos were collected, and 16 GCPs were measured during the UAV overpasses in Menyuan.
- 3) The UAV flight altitude was set to 100 m, 125 photos were collected, and 9 GCPs were measured during the UAV overpasses in Gangcha.
- 4) The UAV flight altitude was set to 80 m, 1244 photos were collected, and 17 GCPs were measured during the UAV overpasses in Tianjun.

B. Method

Fig. 4 presents a flowchart of the method used for accuracy verification of the ICESat-2/ATL06 product. CORS field

²[Online]. Available: <https://dl.djicdn.com/>

TABLE III
COMPARISON OF THE PARAMETERS USED FOR ICESAT-1/GLAS AND ICESAT-2/ATLAS

Satellite identification	GLAS	ATLAS
Design life	3 years (actually 7 years)	3 years
Track height	590 km	500 km
Orbit inclination	94°	92°
Track type	Non-synchronous	Non-synchronous
Repeat cycle	183 days	91 days
Working start time	2003.01	2018.09
Wavelength	1064 nm and 532 nm	532 nm
Number of beams	1 beam	6 beams
Pulse frequency	40 Hz	10 k Hz
Spot diameter	60-70 m	10-17 m
Repeat cycle	183 days	91 days
High accuracy	0.15 m	0.1 m
Data collection method	Analogue-to-digital conversion	Photon counting

measurements can survey the GCPs of UAV images for aerial triangulation, and thus, be used for 3-D model construction and DEM extraction. GVPs measured by CORS and DEM derived from UAVs were used to verify the vertical accuracy of the elevation product ATL06.

1) *ICESat-2 Altimetry Principle and Data Processing of the ATL06 Product*: Satellite laser altimetry is a space geodesy technology that measures ground elevation from satellite platforms. The transmitting device of an altimeter transmits the modulated compressed pulse to the earth's surface at a certain pulse repetition frequency through the antenna. After ground reflection, the receiver receives the returned pulse and measures the time interval between the transmitted pulse and the received pulse. According to this time interval and the waveform of the return pulse, the distance from the satellite to the ground can be measured [35]. Spaceborne altimeters can be classified as radar altimeters and laser altimeters, and their altimetry principles are often the same. A laser altimeter always operates in the optical remote visible light band at a higher working frequency, but a radar altimeter usually operates in the microwave band, for example, the operating bands of the Sentinel-3 radar altimeter are the C-band and Ku-band. In general, a laser altimeter can provide higher-accuracy surface elevation data than a radar altimeter.

ICESat-1/GLAS is the world's first satellite laser altimetry for earth observation. Compared with GLAS, ICESat-2/ATLAS has made great improvements mainly in four aspects [36], [37].

- 1) The ATLAS positioning error in the horizontal direction is reduced because it uses the track-crossing measurement method and minimizes the influence of the terrain slope, which is less than 6.5 m on the ground.
- 2) The higher frequency and density of ATLAS laser pulses reduce the spot diameter.
- 3) The sun background noises can be effectively removed because ICESat-2 adopts the photon counting method rather than the analog-to-digital data acquisition method.
- 4) Multibeam detection provided by ATLAS greatly improves the efficiency of measurement and shortens the

time required to complete the entire surveying and mapping task. The detailed parameters of the two satellite laser altimeters are described in Table III.

The fast pulse (10 kHz) of the ICESat-2/ATLAS altimeter yields flat disk-shaped photon footprint centers in the direction of the ground track, approximately 50 cm in the vertical direction and 17 m in the horizontal direction, and a distance between the flat disks of 0.7 m. Since most of the earth's land surface is smooth, and the surface slope varies little on a scale below a few hundred meter, the short linear segments (along-track) can approximate the surface profiles measured by ATLAS. Among them, the fixed length of each part is 40 m, and the center distance is 20 m (50% overlap). The ground-return photon events (PEs) identified by the ATL03 product are fitted with sloping line segments, and those that do not capture this fitting process can be treated as surface roughness. Therefore, the mean detected PE height can be derived by the along-track linear fit and across-track polynomial fit.

The ATL06 product provides the surface height related to the WGS-84 ellipsoid at a given time and point on earth's surface, and the formula is as follows:

$$h = (H - R - \Delta R) - H_{\text{geoid}} \quad (1)$$

where $h(m)$ means the standard surface height, which is the segment-center height of the selected PEs. H is the mean surface without considering various offsets, and R indicates the first-photon-bias correction of photon-counting detectors. ΔR means the estimated bias of the fullwave form transmit-pulse mean and waveform is consistent with the received pulse [38]. H_{geoid} is the geoid height. We used the WGS-84 reference system and orthometric heights for CORS GPCPs, and GVPs and this is also the horizontal and vertical datum for the derived DEM. The ICESat-2 altimeter data are in an ellipsoid height, and we need to shift the ICESat-2 altimeter data into an orthometric height by using geoid height. All four parameters on the right-hand side of formula (1) can be directly extracted from the ATL06 data products.

In addition, the data processing of the ATLAS height measurements involves removing incorrect laser point cloud data that are not from the earth's surface. When some photons return from the top of the cloud, the elevation values recorded by ATLAS are shown as being at the top of the cloud instead of the ground. Therefore, we use the Python programming language to pre-process the ATL06 elevation products by eliminating erroneous laser points and extracting the correct surface elevation data.

2) *CORS Survey and UAV Flight*: The CORS system is a high-tech product combining satellite positioning systems, computer network technology, and other technologies. The system mainly consists of five parts: a reference station, data processing center, data transmission system, positioning and navigation data system, and user application system. The CORS measurement is not only convenient and avoids postprocessing calculations, but also has a high positioning accuracy of a few centimeters. The theoretical accuracy is 2 cm horizontally and 3 cm vertically [39]–[41], which can satisfy user accuracy requirements in different industries, such as urban planning, mining surveys, positioning, glacial changes, and other social needs. In addition, for relatively small areas, a UAV is a common tool to generate high-precision surface elevation data with low GSD based on the photogrammetry method, which is used in many disciplines because of its flexibility and many other advantages, such as being unblocked by terrain, low labor requirements, and low cost [42], [43]. RTK GPS/GNSS systems have been available for well over a decade and can provide quick and accurate point measurements [44]. In this article, CORS is used to measure GCPs for adjusting the photography beam obtained from a UAV DEM. After constructing an aerial triangulation network, the DEM can be extracted based on the real 3-D model of the surface.

3) *UAV DEM Extraction*: In this research, CORS GVP measurements and high-resolution DEMs derived from UAVs are used to evaluate the vertical accuracy of the ICESat-2/ATL06 product. The CORS measurement method is relatively simple, and the key lies in the design of the GVP measurement sample, which will be described in detail later. Therefore, how to use UAV imagery to obtain high-precision DEMs has become the key step.

In this study, we use DJI Phantom4 RTK to collect images of four experimental areas by selecting flight parameters such as altitude and image overlap. The photogrammetric software system DPGrid developed by the Wuhan University was selected to process irregular and overlapping aerial image data, generate georeferenced 3-D point cloud images, and finally generate a DEM (see Fig. 4). Its main input datasets include UAV camera parameters, flight images, position and orientation system (POS), and GCPs. Although the theoretical positioning accuracy of the DJI Phantom4 RTK can reach 10 cm, the RTK communication is unstable when the UAV is flying. Therefore, the actual POS information of each image is not accurate, and needs GCPs to improve its position and orientation accuracy.

The specific processing flow consists of four steps [45]: data preparation, aerial triangulation, 3-D model construction, and DEM generation/editing (see Fig. 4).

1) Data preparation includes obtaining UAV original image data, camera calibration parameters, flight parameters,

and GCPs. GCPs were measured using the CORS GPS measurements before the flight, and the color and size of the GCP ground marks must be distinguishable from the natural colors of the study area.

2) Aerial triangulation is the most important and complex step of DEM extraction, and can establish relationships between the imagery coordinate systems and a defined geodetic coordinate system. Aerial triangulation includes the interior, relative, and absolute ordination, which can finally compute the precise and accurate POS data of individual images in the moment of drone photography by using the GCPs and tie points among a series of overlapping aerial photographs.

3) After aerial triangulation, the 3-D model construction can be constructed in the DPGrid photogrammetry system.

4) The DEM can be derived from the photogrammetric stereo model established by image matching technology. The generated DEM is edited, and the orthophoto images are output. The CORS measurements and the UAV DEM were both under the WGS84 ellipsoid. UAV orthophoto images and ICESat-2/ATL06 plot locations of the four experimental areas are shown in Fig. 5.

4) *Field Sample Design for CORS GVPs*: Since photogrammetry is a surface-measured method, the UAV-based photogrammetry method can ensure that the ATLAS laser footprints must pass through the UAV-derived DEM. However, CORS GPS measurement is a point measurement, and the measured CORS readings cannot truly describe the corresponding elevation values of laser points of the verified altimetry satellite according to the (X, Y) coordinate recorded by the ICESat-2/ATL06 footprints. Therefore, it is necessary to set up some surface-like sample areas in the study area to intensively measure a large amount of CORS data in each sample area to ensure that the CORS data can correspond to the ICESat-2 altimetry data well.

Therefore, many CORS measurement samples (see Fig. 6) in the four experimental areas were designed with the help of survey tools, such as a tape measure, rope, nails, and recording paper. Considering the ICESat-2 horizontal positioning error range (< 6.5 m) [20], the side length of the field sample for quadrilateral squares requirements is greater than 6.5 m. In general, there are three main steps in field sample design: stake out the ICESat-2 footprint position, determine the quadrats with the corresponding footprints center, and measure several CORS points in the quadrats. Here, we take Qinggangxia as an example to illustrate the design quadrants, as shown in Fig. 6. First, the spatial location of the ICESat-2 laser point that needs accuracy verification was found with the stakeout function of the CORS GPS receiver by inputting the (X, Y) coordinate of the ICESat-2/ATL06 footprint. Second, a sample square of approximately 8×8 m around the footprint recently geolocated was determined by four iron sets and a rope. Third, more than three CORS points were measured in each field sample; thus, their average elevation value was calculated as the GVP value for accuracy verification.

5) *Elevation Accuracy Analysis*: In this article, the values of the *in situ* CORS GVPs and UAV DEM can be considered to be reasonable “true” surface elevations, and were selected for

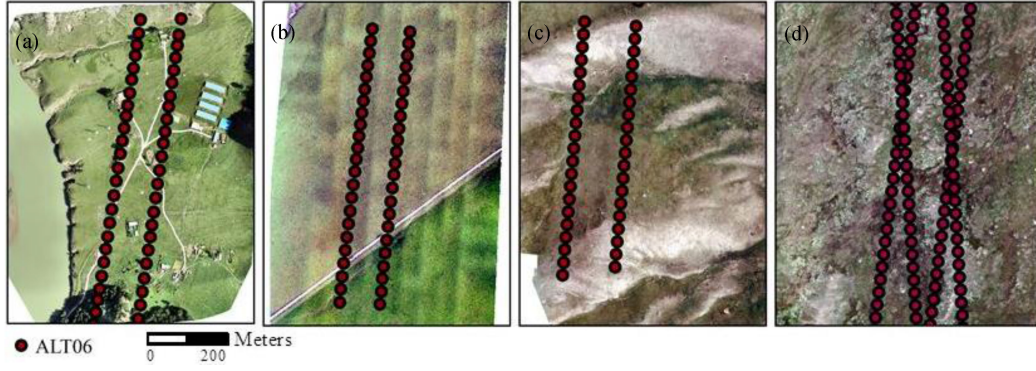


Fig. 5. UAV orthophoto images and ICESat-2/ATL06 plot locations of the four experimental areas. (a) Qinggangxia. (b) Menyuan. (c) Gangcha. (d) Tianjun.

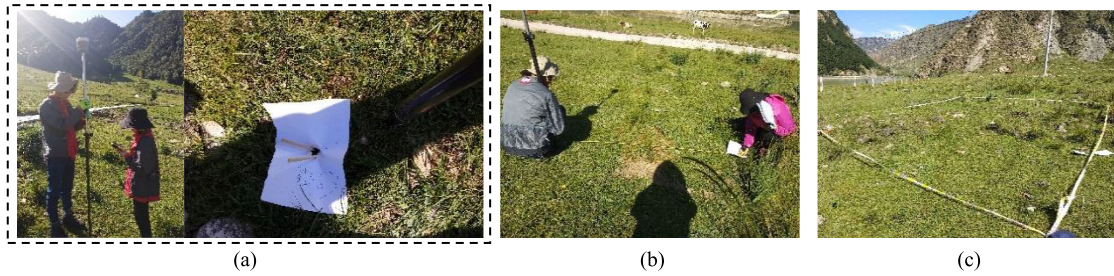


Fig. 6. Three steps of the field sample design for CORS GVPs. (a) Geolocate the ICESat-2 footprint. (b) Determine the sample quadrats with the corresponding footprint center. (c) Measure several CORS points in the field sample.

the quantitative assessment of the accuracy of surface elevation recorded by the ICESat-2/ATL06 product. Three statistical indicators were selected for vertical accuracy evaluation, including the mean bias error (MBE), the root-mean-square difference (RMSE), and the square of the coefficient of determination (R^2 , ranging from 0 to 1). The formulas for these statistics are as follows:

$$MBE = \frac{1}{n} \sum_{i=1}^n (M_i - X_i) \quad (2)$$

$$RMSE = \sqrt{\frac{1}{n} \sum_{i=1}^n (M_i - X_i)^2} \quad (3)$$

$$R^2 = \left(\frac{\sum_{i=1}^n (X_i - \bar{X})(M_i - \bar{M})}{\sqrt{\sum_{i=1}^n (X_i - \bar{X})^2} \sqrt{\sum_{i=1}^n (M_i - \bar{M})^2}} \right)^2 \quad (4)$$

where M_i is the ICESat-2/ATL06 values and X_i is the observations, which are the measured elevation values of the CORS GVPs or the UAV DEM. \bar{M} and \bar{X} represent the averages of the measured data and satellite altimetry data, respectively, and n is the number of samples. The RMSE is sensitive to the estimation error and can reflect the difference between the satellite value and the actual value. The MBE provides information about the long-term performance; the smaller the absolute values of the RMSE and MBE are, the higher the accuracy of the ICESat-2/ATL06 product.

IV. RESULT

A. CORS Accuracy Verification

To ensure whether an ICESat-2 photon arrived in each field sample, many CORS points must be measured around the laser spot. After eliminating the anomalous ATL06 footprints in the four experimental areas, 50 CORS GVPs used for verifying satellite altimetry were obtained in 50 sample areas by measuring 348 CORS readings, as described in Table IV.

Based on the definitions of MBE, RMSE, and R^2 in this experiment, the accuracy verification results of the ICESat-2/ATL06 product can be calculated using the CORS GVPs mentioned above (Table IV). The statistical results show that the satellite altimeter ATLAS of ICESat-2 can measure the surface elevation value with high accuracy, and the MBE and RMSE are -0.0081 and 0.0847 m between the ATL06 estimates and CORS measurements, respectively, with an R^2 close to 1. It is worth noting that the terrain can affect the precision of the laser spot measurement. Compared with the other three relatively flat areas, Gangcha has a lower elevation accuracy, the MBE is -0.0733 m, and the RMSE is 0.1112 m. Specific detailed accuracy statistical indicators are described in Table V.

B. UAV Accuracy Verification

Using the DEM editing function of the photogrammetric 3-D surface models, high-precision DEM data with a 0.03-m GSD were generated. As shown in Fig. 7, a total of 208 satellite

TABLE IV
BASIC INFORMATION OF ICESAT-2/ATL06 AND CORS GVPs FOR FIELD SAMPLES IN THE EXPERIMENTAL AREAS

Experimental areas	Elevation of the ICESat-2/ATL06 footprints (m)	CORS		Height difference (m)
		Number of GVPs	CORS mean values in the plot (m)	
Qinggangxia	2362.5221	26	2362.4432	0.0789
	2360.8150	10	2360.7710	0.0440
	2357.7969	8	2357.7160	0.0809
	2350.8022	8	2350.7285	0.0737
	2347.8677	7	2347.8279	0.0398
	2354.4642	7	2354.3438	0.1204
	2357.7978	6	2357.8709	-0.0731
	2356.8374	6	2356.9212	-0.0838
	2358.0559	5	2358.1520	-0.0961
	2349.6487	4	2349.7990	-0.1503
	2353.0666	4	2352.9922	0.0744
	2358.0559	4	2358.0245	0.0314
	2363.0122	3	2362.9425	0.0697
	3203.6893	10	3203.7053	-0.0160
	3193.9443	10	3193.8167	0.1276
Menyuan	3181.9886	9	3181.8945	0.0941
	3195.5247	8	3195.6032	-0.0785
	3198.5630	8	3198.6411	-0.0781
	3200.9620	8	3200.8261	0.1359
	3193.7112	8	3193.8228	-0.1116
	3189.5986	8	3189.6192	-0.0206
	3188.4822	8	3188.3082	0.1740
	3197.1125	4	3196.9501	0.1624
	3193.6523	4	3193.8238	-0.1715
	3191.6970	4	3191.6573	0.0397
	3188.2181	3	3188.2341	-0.0160
	3201.2133	3	3201.2741	-0.0608
	3425.08865	22	3425.2170	-0.1284
	3416.7663	8	3416.9083	-0.1420
	3391.1530	6	3391.2351	-0.0821
Gangcha	3420.2635	4	3420.1533	0.1102
	3410.3241	4	3410.4732	-0.1491
	3424.1090	3	3424.1432	-0.0342
	3388.8838	3	3388.9711	-0.0873
	3435.4617	10	3435.5112	-0.0495
Tianjun	3444.9677	10	3445.0231	-0.0554
	3445.1709	8	3445.1706	0.0003
	3445.3228	8	3445.3101	0.0127
	3440.3540	8	3440.3541	-0.0001
	3440.3389	8	3440.4139	-0.0750
	3441.1792	8	3441.1926	-0.0134
	3441.1716	8	3441.2135	-0.0419
	3440.3472	8	3440.3502	-0.0030
	3440.1715	8	3440.1832	-0.0117
	3440.0845	4	3440.1198	-0.0353
	3445.0354	4	3445.0605	-0.0251
	3440.6577	4	3440.6525	0.0052
	3445.0166	3	3445.0380	-0.0214
	3445.0593	3	3445.0063	0.0530
	3439.9976	3	3440.0169	-0.0193

TABLE V
BASIC STATISTICAL INDICATORS OF ICESat-2/ATL06 COMPARED WITH THE CORS READINGS

Experimental areas	MBE (m)	RMSE (m)	R^2
Qinggangxia	0.0161	0.0840	0.9997
Menyuan	0.0129	0.1071	0.9998
Gangcha	-0.0733	0.1112	0.9999
Tianjun	-0.0174	0.0344	0.9999
Total	-0.0081	0.0846	0.9999995

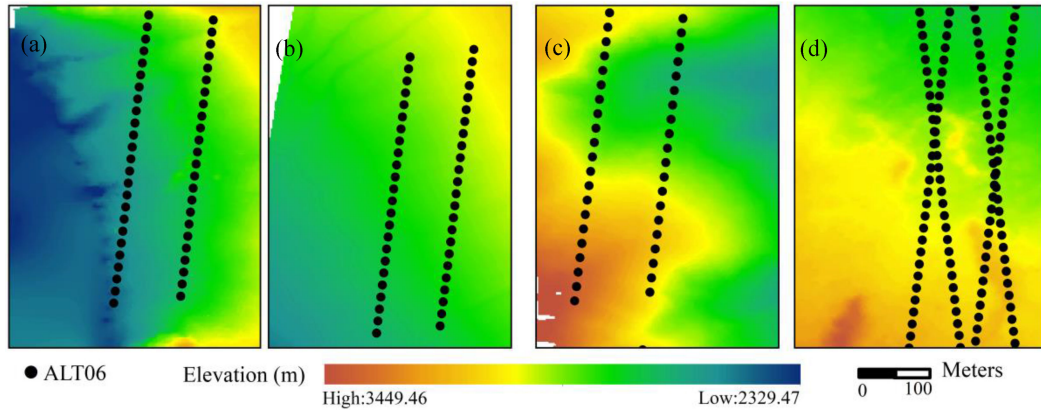


Fig. 7. UAV DEM images and ICESat-2/ATL06 footprint point locations of the four experimental areas. (a) Qinggangxia. (b) Menyuan. (c) Gangcha. (d) Tianjun.

TABLE VI
BASIC STATISTICAL INDICATORS OF ICESat-2/ATL06 COMPARED WITH THE UAV DEM

Experimental areas	MBE (m)	RMSE (m)	R^2
Qinggangxia	0.0004	0.1314	0.9998
Menyuan	0.0392	0.1438	0.9999
Gangcha	-0.0575	0.1891	0.9999
Tianjun	0.0306	0.1441	0.9988
Total	0.0094	0.1517	0.9999999

altimetry laser points passed through four experimental areas, 40 footprints are in Qinggangxia, 48 footprints are in Menyuan, 41 footprints are in Gangcha, and 79 footprints are in Tianjun.

To use the DEMs generated by a UAV to verify the accuracy of the ICESat-2/ATL06 product, the corresponding DEM elevation values for each pixel in the 208 laser footprints were extracted according to the bilinear interpolation method. The detailed statistical indicators of ICESat-2/ATL06 with the UAV DEM are described in Table VI, and the total MBE, RMSE, and R^2 values are 0.0094, 0.1517 m, and close to 1, respectively. Similar to the CORS verification results mentioned above, the ATL06 measurements of the Gangcha area with complicated terrain have lower accuracy, although ICESat-2 greatly reduced the impact of the slope. Compared with the field CORS measurements, the accuracy of ICESat-2/ATL06 with the UAV DEM is slightly lower, which may be subject to the accuracy of DEM extraction by UAV photogrammetry.

Field data are generally limited due to differences in methodologies. As shown in Fig. 8, in general, regardless of whether the CORS survey or UAV mapping is used for verification, the ATL06 satellite altimetry product can correctly collect the laser footprints corresponding to the surface and retrieve surface elevation even over complex surfaces in the Qilian Mountains area, although the accuracy varies with different regions or terrains.

V. DISCUSSION

A. Geolocation Accuracy

To ensure that the CORS measurements can verify the elevation of the laser spot, 50 samples were designed in this experiment, and more than 3 CORS points were measured in each sample area. The statistical results show that the satellite

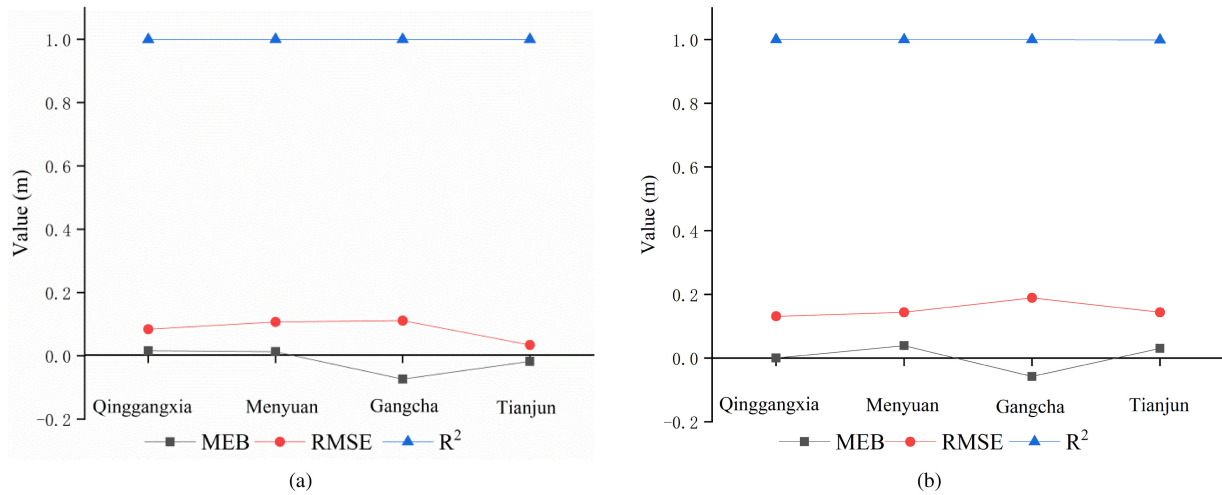


Fig. 8. Basic statistical indicators of ICESat-2/ATL06 compared with the UAV DEM and CORS readings. (a) CORS. (b) UAV DEM.

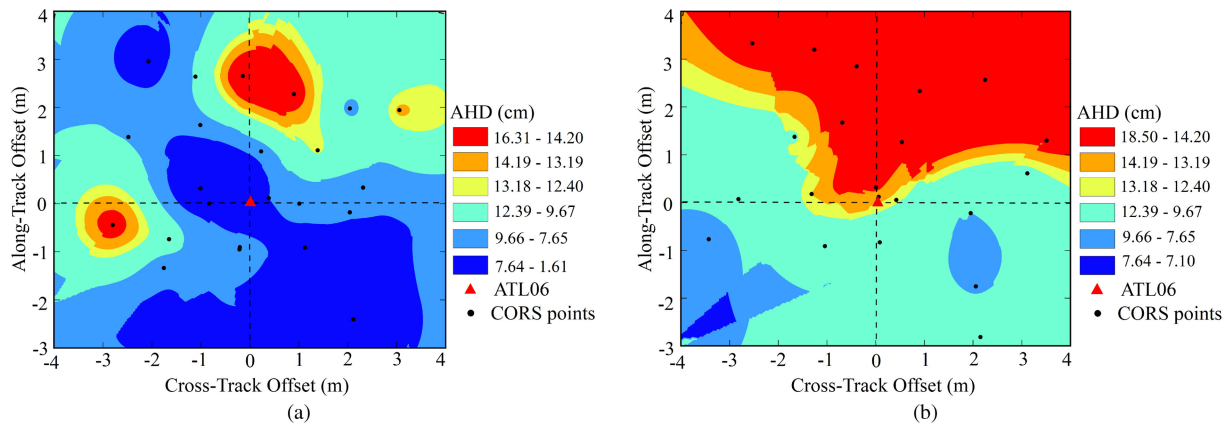


Fig. 9. Geolocation distribution of the ICESat-2 points compared with the CORS points in two special field areas. (a) Qinggangxia. (b) Gangcha.

altimetry products have very high vertical accuracy. However, the positioning error characteristics of the plane position of the ICESat-2/ATL06 laser point need further analysis in the sample area. It is well known that the horizontal accuracy of ICESat-2 data is related to factors such as satellite orbit position uncertainties and pointing determination error. The CORS measurements are considered to be the “true” surface height value of the ground position and can accurately evaluate both the horizontal and vertical accuracies of ATLAS geolocated footprints.

Ultimately, two special field samples (8×8 m) with dense ground CORS observations (more than 20) were constructed to specifically explore the positioning error distribution of ICESat-2 laser spots in Qinggangxia and Gangcha. The large sample size of Qinggangxia was located over grassland with a relatively flat terrain (slope of 8.9°), and 26 CORS points were distributed in this area. The Gangcha sample is located on a steep slope of 20.2° , and there are 22 CORS measurements.

In the process of kriging interpolation in this study, the variable type of interpolation is selected as a semivariation function, and the interpolation model is an exponential function. The results of ordinary kriging interpolation are shown in Fig. 9.

Kriging interpolation is performed for the absolute height difference (AHD) of discrete points between CORS readings and ATL06 values along the cross-track and along-track directions in the two large sample areas. Fig. 9 shows that the AHD value at the laser spot is small, which indicates that the ATL06 laser spot positioning is generally more accurate. However, the spatial distribution of the AHD also shows that the centroid location of the laser spot is affected by the slope, and the larger the slope is, the lower the geolocation accuracy for an ICESat-2 track over the Qilian Mountains [see Fig. 9(b)].

B. Sensitivity Analysis of Elevation Accuracy With Surface Slope

The abovementioned analysis shows that the terrain has an important influence on the accuracy of the ICESat-2/ATL06 product. It is necessary to explore the relationship between the elevation accuracy and the surface slope for the laser point elevation recorded by ICESat-2 in the study area. The slope at all laser point locations is taken from the UAV DEM. The absolute differences between ICESat-2 elevation values and CORS

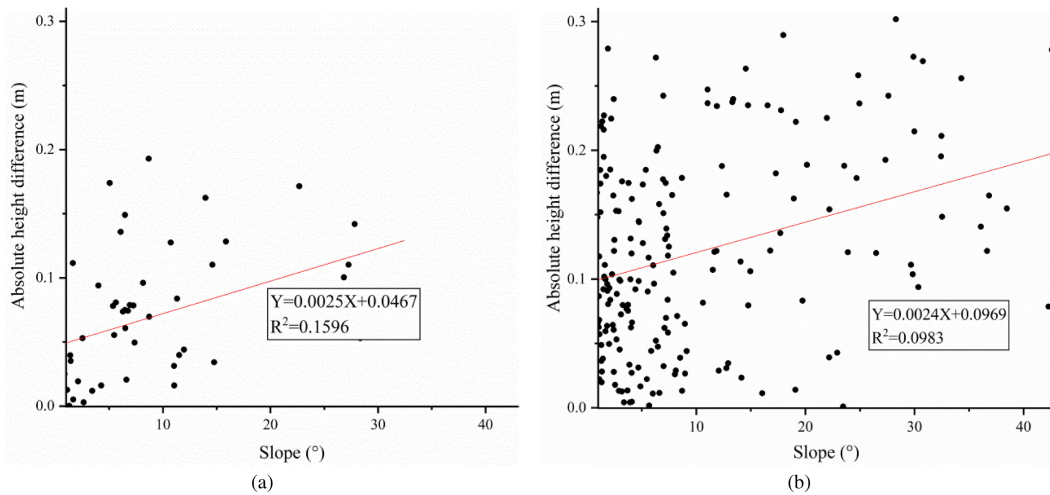


Fig. 10. Scatterplots of the AHD between the elevations of ICESat-2/ATL06 and CORS or the UAV DEM versus the slope. (a) CORS. (b) UAV DEM.

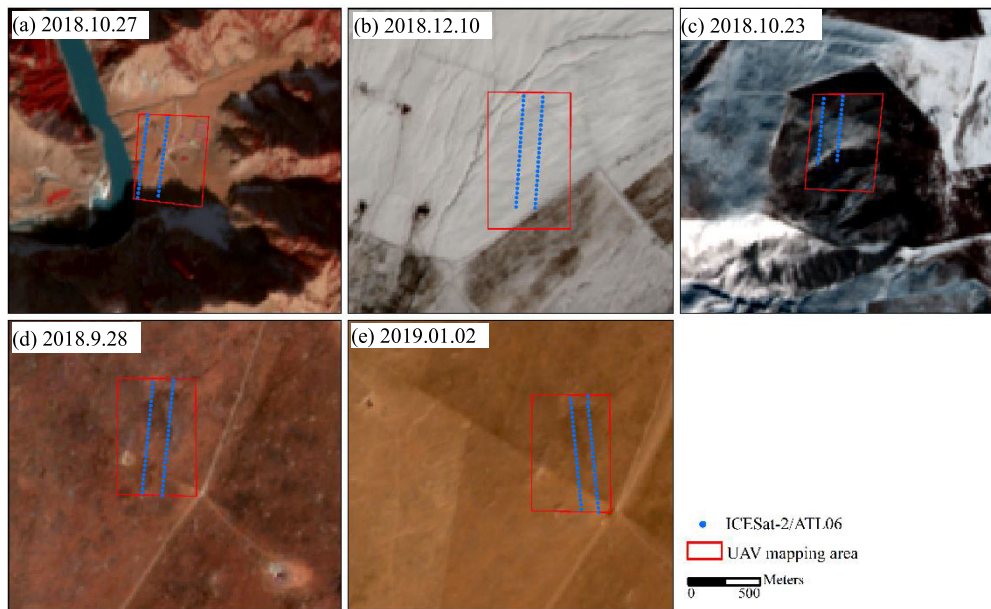


Fig. 11. False-color composites (RGB: bands 8, 4, 3) of Sentinel-2 MSI images closest to the ICESat-2 overpass time. (a) Qinggangxia. (b) Menyuan. (c) Gangcha. (d) and (e) Tianjun.

observations or UAV DEM elevations at these satellite laser positions were calculated. The results in Fig. 10 show that the high difference between the ICESat-2/ATL06 data and CORS measurements is between 0 and 0.17 m. The AHD between the UAV data and ICESat-2/ATL06 data is between 0 and 0.27 m. Fig. 10(a) indicates that where the terrain is relatively flat ($<10^\circ$), the height difference is concentrated below 0.2 m, and where the slope is greater than 15° , the height difference is concentrated within approximately 0.1–0.27 m. For the CORS data [see Fig. 10(b)], the height difference is concentrated below 0.10 m when the terrain is relatively flat ($<10^\circ$); when the slope is greater than 15° , the height difference is concentrated within approximately 0.1–0.15 m. Overall, the satellite has largely improved the impact of topography on these data by increasing

the sampling frequency and cross measurement. However, as shown in Fig. 10, in places with large slope changes, the data are minimally affected (CORS: $R^2 = 0.1596$; UAV DEM: $R^2 = 0.0938$).

C. Sensitivity of Elevation Accuracy to Changes in Land Cover Types

In this experiment, as described in Table II, the times of CORS field measurements and UAV mapping are inconsistent with the transit time of ICESat-2. It may be questioned whether there will be problems with vertical elevation accuracy errors caused by variations in land cover types. To demonstrate the effects of land cover types on height recovery, five scenes of the Sentinel-2

MSI (MultiSpectral Instrument) images closest to the ICESat-2 overpass time were downloaded, as depicted in Fig. 11.

The results have shown that changes in land cover type have little effect on accuracy verification in the study areas. First, the spectral variation in land cover from the optical images is mainly caused by different seasons, and the surface vegetation grew vigorously during this field verification experiment. Except for the Menyuan and Gangcha areas, due to the relatively low local temperature at the ICESat-2 overpass time, the land vegetation degraded and appeared as dark red to yellowish tones in the false-color composite images. In Menyuan Gangcha, according to the local weather observation records,³ light snow only started on the day of satellite transit, and the snow thickness was small and had almost no effect on the ground elevation.

D. Limitations of Experiments

In this article, we use field surveys of CORS and UAV DEMs to verify the elevation accuracy of the ICESat-2/ATL06 product. However, there are some experimental limitations when conducting experiments. First, it is unavoidable that there is a time interval between the data measurement and the acquisition of ICESat-2/ATL06 data. It is well known that the revisit time of ICESat-2 is currently 91 days. Therefore, the time interval between the data measurement and ICESat-2 overpass is months (see Table II). During the time interval, the surface may change slightly in response to changes in the season.

In addition, this experiment only considered bare land and grassland, and did not consider woodland, glaciers, and other landform types (see Table I). Moreover, the laser wavelength of the ICESat-2 ATLAS sensor is 532 nm, which makes it possible to be obstructed by clouds. In this case, no photons, or only very few photons, can reach the land surface when there are clouds. Therefore, only a small portion of the ICESat-2 data is suitable for land surface monitoring in the presence of clouds.

VI. CONCLUSION

The newly launched laser altimeter satellite ICESat-2 provides reliable data for many applications, such as surface elevation change monitoring and the comprehensive estimation of lake and canopy heights. The primary scientific objectives of ICESat-2 are focused on the cryosphere; however, a range of measurements are collected globally over all surface types, including forests, oceans, lakes, and land. According to official satellite information, the ATL06 product can accurately estimate surface elevation even under moderately (optical thickness of <2) cloudy conditions.

The purpose of this article is to verify the elevation accuracy of the ICESat-2 ATL06 land product by comparing 208 laser footprints returned from the ground surface from four sample locations using high-precision CORS GVP measurements and UAV mapping technology in the Qilian Mountains. Quantitative results show that the laser height measurement product ATL06 has very high vertical accuracy and horizontal positioning accuracy. Overall, the vertical accuracy of altimetry data evaluated

by CORS measurement is high ($MBE = -0.0081$ m; $RMSE = 0.0846$ m), while the vertical accuracy of altimetry data evaluated by UAV DEM verification is slightly lower ($MBE = -0.0094$ m; $RMSE = 0.1517$ m), but the MBE values are all within 0.01 m, and the values of the RMSEs are all within 0.2 m. It should be noted that one of the reasons for the low accuracy of the UAV verification is the accuracy of the UAV DEM data extraction.

Furthermore, the ICESat-2 horizontal positioning accuracy was discussed using two special large sample areas with a high number of CORS observations. However, the test results found that, regardless of the vertical accuracy or the laser spot positioning accuracy, all the values of ATL06 were affected by the terrain slope. In general, when the terrain slope is less than 10° , the vertical accuracy error of the ATL06 product is small and tends to be stable; however, when the terrain slope is greater than 20° , the accuracy of the satellite altimetry product decreases as the slope increases (see Fig. 10). In fact, the ATL06 product accuracy of surface elevations is limited by the geolocation accuracy of the footprints.

Besides, in this article, the traditional elevation accuracy verification method is applied. The 3-D coregistration is an important means to compare the elevation errors of different DEM data [46]. Shean *et al.* [47] proposed a coregistration tool, the demcoreg package, for 3-D co-registration, which had been applied in the study of glacier changes [48]. In the next step, residual coregistration errors will be considered to further improve the accuracy of the verification by using the 3-D coregistration of point cloud to the DEM function of the demcoreg package.

ACKNOWLEDGMENT

The ICESat-2 data were obtained from the NSIDC (<https://icesat-2.gsfc.nasa.gov/>). Yanli Zhang designed the research, formulated the experiment, and revised the article. Yan Pang helped with the experiments and wrote the article. Dudu Cui operated the UAV for photography, and Yupeng Ma and Linhong Chen designed the field samples and took the CORS measurements. All authors contributed to the discussion of the results.

REFERENCES

- [1] H. J. Zwally *et al.*, "ICESat's laser measurements of polar ice, atmosphere, ocean, and land," *J. Geodynamics*, vol. 34, no. 3, pp. 405–445, 2002.
- [2] A. Kääb *et al.*, "Brief communication: contending estimates of 2003–2008 glacier mass balance over the Pamir–Karakoram–Himalaya," *Cryosphere*, vol. 9, pp. 557–564, 2015.
- [3] J. M. Sirota *et al.*, "The transmitter pointing determination in the geoscience laser altimeter system," *Geophysical Res. Lett.*, vol. 32, pp. 1–4, 2005.
- [4] H. J. Zwally *et al.*, "ICESat's laser measurements of polar ice, atmosphere, ocean, and land," *J. Geodynamics*, vol. 34, no. 3–4, pp. 405–445, 2002.
- [5] M. Alberti and D. Biscaro, "Height variation detection in polar regions from ICESat satellite altimetry," *Comput. Geosci.*, vol. 36, no. 1, pp. 1–9, 2010.
- [6] C. Gao *et al.*, "A joint inversion estimate of Antarctic ice sheet mass balance using multi-geodetic data sets," *Remote Sens.*, vol. 11, no. 6, pp. 1–23, 2019.
- [7] J. B. Zong, Q. H. Ye, and L. D. Tian, "Recent naimona'nyi glacier surface elevation changes on the Tibetan plateau based on ICESat/GLAS, SRTM DEM and GPS measurements," *China Sci. Bull.*, vol. 59, pp. 2108–2118, 2014.

³ [Online]. Available: http://tianqi.2345.cn/wea_history/71194.html

- [8] B. E. Schutz *et al.*, "Overview of the ICESat mission," *Geophysical Res. Lett.*, vol. 32, no. 21, pp. 1–4, 2005.
- [9] J. DiMarzio *et al.*, "GLAS/ICESat 500 m laser altimetry digital elevation model of Antarctica," National Snow and Ice Data Center. Digital media, Boulder, CO USA, 2007.
- [10] A. Braun and G. Fotopoulos, "Assessment of SRTM, ICESat, and survey control monument elevations in Canada," *Photogrammetric Eng. Remote Sens.*, vol. 73, no. 12, pp. 1333–1342, 2007.
- [11] X. P. Du *et al.*, "Vertical accuracy assessment of SRTM and ASTER GDEM over typical regions of China using ICESat/GLAS," *Earth Sci.-J. China Univ. Geosciences*, 2013, no. 04, pp. 229–239.
- [12] D. D. Yavaşlı, "Estimation above ground forest biomass at muğla using ICESat/GLAS Landsat data," *Remote Sens. Appl., Soc. Environ.*, vol. 4, pp. 211–218, 2016.
- [13] I. Indirabai *et al.*, "Estimation of forest structural attributes using ICESat/GLAS-Spaceborne laser altimetry data in the western ghats region of India," *J. Geovisualization Spatial Anal.*, vol. 3, no. 2, 2019, Art. no. 10.
- [14] F. Zou *et al.*, "Water storage variations in Tibet from GRACE, ICESat, and hydrological data," *Remote Sens.*, vol. 11, no. 9, pp. 1–23, 2019.
- [15] J. Van Den Hoek *et al.*, "Monitoring reservoir drought dynamics with landsat and radar/lidar altimetry time series in persistently cloudy eastern Brazil," *Remote Sens.*, vol. 11, no. 7, pp. 1–24, 2019.
- [16] B. E. Schutz *et al.*, "Overview of the ICESat mission," *Geophysical Res. Lett.*, vol. 32, no. 21, pp. 1–4, 2005.
- [17] National Snow and Ice Data Center. Boulder, CO, USA, 2019. Accessed on: May 28, 2019. [Online]. Available: https://nsidc.org/ATL08_20190212052542_06990206_r001
- [18] B. Smith *et al.*, "Land ice height-retrieval algorithm for NASA's ICESat-2 photon-counting laser altimeter," *Remote Sens. Environ.*, vol. 233, pp. 111–352, 2019.
- [19] A. L. Neuenschwander and K. Pitts, "The ATL08 land and vegetation product for the ICESat-2 mission," *Remote Sens. Environ.*, vol. 221, pp. 247–259, 2019.
- [20] G. D. Chen *et al.*, "Determination of sea ice freeboard in Arctic from ICESat: Case study of 2005–2006," *Acta Geodaetica et Cartographica Sinica*, vol. 44, no. 6, pp. 625–633, 2015.
- [21] G. Zhang *et al.*, "Tibetan plateau's lake level and volume changes from NASA's ICESat/ICESat-2 and Landsat missions," *Geophysical Res. Lett.*, vol. 46, no. 22, pp. 13107–13118, 2019.
- [22] A. L. Neuenschwander and L. A. Magruder, "Canopy and terrain height retrievals with ICESat-2: A first look," *Remote Sens.*, vol. 11, no. 14, pp. 1–13, 2019.
- [23] J. Li B., "Comparison of GPS and traditional measurement techniques in geological exploration," *Geospatial Inf.*, vol. 9, no. 03, pp. 56–57+188, 2011.
- [24] G. B. Jia *et al.*, "The influence and precision analysis on RTK measure to tradition geodetic mapping method," *Geomatics Spatial Inf. Technol.*, vol. 40, no. 04, pp. 162–165, 2017.
- [25] M. F. Yuan and Z. L. Xie, "Analysis of measurement accuracy and influence factors of network RTK based on CORS," *Geomatics Spatial Inf. Technol.*, vol. 43, no. 7, pp. 31–44, 2020.
- [26] W. Wester-Ebbinghaus, "Aerial photography by radio controlled model helicopter," *Photogrammetric Rec.*, vol. 10, no. 55, pp. 85–92, 2006.
- [27] B. Ruzgienė *et al.*, "The surface modelling based on UAV photogrammetry and qualitative estimation," *Measurement*, vol. 73, pp. 619–627, 2015.
- [28] U. Niethammer, S. M.R. James, and J. Rothmund, "UAV-based remote sensing of the super-sauze landslide: Evaluation and results," *Eng. Geol.*, vol. 128, pp. 2–11, 2012.
- [29] J. S. Aber, I. Marzolf, and J. B. Ries, *Small-Format Aerial Photography: Principles Techniques and Geoscience Applications*. San Diego, CA, USA: Elsevier Science, 2010.
- [30] B. Kršák *et al.*, "Use of low-cost UAV photogrammetry to analyze the accuracy of a digital elevation model in a case study," *Measurement*, vol. 91, pp. 276–287, 2016.
- [31] Q. Feng *et al.*, "UAV remote sensing for urban vegetation mapping using random forest and texture analysis," *Remote Sens.*, vol. 7, no. 1, pp. 1074–1094, 2015.
- [32] A. S. Laliberte *et al.*, "Acquisition, orthorectification, and Object-based classification of unmanned aerial vehicle (UAV) imagery for range-land monitoring," *Photogrammetric Eng. Remote Sens.*, vol. 76, no. 6, pp. 661–672, 2010.
- [33] X. Li *et al.*, "Tightening ecological management facilitates green development in the Qilian mountains," *Chin. Sci. Bull.*, vol. 64, no. 27, pp. 176–185, 2019.
- [34] B. Smith *et al.*, "Land ice height-retrieval algorithm for NASA's ICESat-2 photon-counting laser altimeter," *Remote Sens. Environ.*, vol. 233, 2019, Art. no. 111352.
- [35] C. L. Cui *et al.*, "The summary of the latest developments of foreign laser altimetry satellite ICESat-2," *Sci. Surveying Mapping*, vol. 10, no. 40, pp. 129–131, 2015.
- [36] W. Abdalati *et al.*, "The ICESat-2 laser altimetry mission," *Proc. IEEE*, vol. 98, no. 5, pp. 735–751, May 2010.
- [37] T. Markus *et al.*, "The ice, cloud, and land elevation Satellite-2 (ICESat-2): Science requirements, concept, and implementation," *Remote Sens. Environ.*, vol. 190, pp. 260–273, 2017.
- [38] B. E. Smith *et al.*, "ICESat-2 algorithm theoretical basis document (ATBD) for land ice along-track height (ATL06)," Appl. Phys. Lab., Univ. Washington, Seattle, WA, USA, 2019. [Online]. Available: <https://icesat-2.gsfc.nasa.gov/science/data-products>
- [39] L. L. Ma *et al.*, "Changes in area and ice reserves of anti-thermal glaciers in the middle of the Himalayas," *China Sci. Bull.*, vol. 18, pp. 22–30, 2010.
- [40] Y. Zhang *et al.*, "Thinning and shrinkage of Laohugou No. 12 glacier in the western Qilian mountains, China, from 1957 to 2007," *J. Mountain Sci.*, vol. 9, no. 3, pp. 343–350, 2012.
- [41] P. Y. Wang *et al.*, "Ice surface-elevation changes of glacier No. 4 of Sigong river in Bogda, Tianshan mountains, during the last 50 years," *Arid Land Geogr.*, vol. 03, pp. 88–94, 2011.
- [42] B. Ruzgienė *et al.*, "The surface modelling based on UAV photogrammetry and qualitative estimation," *Measurement*, vol. 73, pp. 619–627, 2015.
- [43] U. Niethammer *et al.*, "UAV-based remote sensing of the super-sauze landslide: Evaluation and results," *Eng. Geol.*, vol. 128, pp. 2–11, 2012.
- [44] L. Chen *et al.*, "Prediction of spatial distribution of topsoil organic matter content in cultivated land using Kriging methods," *Arid Zone Res.*, vol. 34, no. 04, pp. 798–805, 2017.
- [45] C. C. Li *et al.*, "Quick image-processing method of UAV without control points data in earthquake disaster area," *Trans. Nonferrous Met. Soc. China*, vol. 21, no. supp-S3, pp. s523–s528, 2011.
- [46] C. Nuth and A. Kääb, "Co-registration and bias corrections of satellite elevation data sets for quantifying glacier thickness change," *Cryosphere*, vol. 5, no. 1, pp. 271–290, 2011.
- [47] D. E. Shean *et al.*, "An automated, open-source pipeline for mass production of digital elevation models (DEMs) from very-high-resolution commercial stereo satellite imagery," *ISPRS J. Photogrammetry Remote Sens.*, vol. 116, no. Jun., pp. 101–117, 2016.
- [48] D. Shean *et al.*, "A systematic, regional assessment of high mountain Asia glacier mass balance," *Frontier Earth Sci.*, vol. 7, 2020, Art. no. 363.



Yanli Zhang (Senior Member, IEEE) received the B.E. degree in photogrammetry and remote sensing from Wuhan University, Wuhan, China, in 1999, the M.S. degree in cartography and geographic information system from Lanzhou Jiaotong University, Lanzhou, China, in 2007, and the Ph.D. degree in cartography and geographic information system from the Cold and Arid Regions Environmental and Engineering Institute, Chinese Academy of Sciences, Lanzhou, China, in 2014.

She is currently an Associate Professor with the College of Geography and Environment Science, Northwest Normal University, Lanzhou, China. Her research interests include photogrammetry and quantitative remote sensing and applications.



Yan Pang received the B.S. degree in geographical science major from Lanzhou City University, Lanzhou, China, in 2018. She is currently working toward the M.S. degree in environmental engineering with the Northwest Normal University, Lanzhou, China.

Her research interests include elevation change of glacier and satellite altimetry.



Dudu Cui received the B.S. degree in human geography and urban and rural planning from Shangluo University, Shangluo, China, in 2017, the M.S. degree in cartography and geographic information system from Northwest Normal University, Lanzhou, China, in 2020.

His research interests include quantitative remote sensing and applications.



Yupeng Ma received the B.S. degree in geographical science major from Lanzhou City University, Lanzhou, China, in 2019. He is currently pursuing the M.S. degree in cartography and geographic information system with the Northwest Normal University, Lanzhou, China.

His research interests include remote sensing, snow information extraction, and the application of Sentinel-2 data.



Linhong Chen (Member, IEEE) received the B.S. degree in human geography and urban and rural planning from the School of Geography and Resource Science, Neijiang Normal University, Neijiang, China, in 2018. She is currently working toward the M.S. degree in cartography and geographic information system with the Northwest Normal University, Lanzhou.

Her research interests main about temporal extrapolation for shortwave solar radiation and topographic correction.